Supporting Information File

PD1 blockade potentiates the therapeutic efficacy of photothermally-activated and MRI-guided low temperature-sensitive magnetoliposomes

Guanglong Ma,[a†] Nina Kostevšek,[b†] Ilaria Monaco,[c] Amalia Ruiz,[a] Boštjan Markelc,[d] Calvin C. L. Cheung,[a] Samo Hudoklin,[e] Mateja E. Kreft,[e] Hatem A.F.M Hassan,[a] Matthew Barker,[a] Jamie Conyard, [f] Christopher Hall, [f] Stephen Meech,[f] Andrew G. Mayes, [f] Igor Serša,[g] Maja Čemažar,[d] Katarina Marković,[h] Janez Ščančar,[h] Mauro Comes Franchini,[c] and Wafa T. Al-Jamal [a]*

† Both authors equally contributed to this manuscript

[a] School of Pharmacy, Queen's University Belfast, Belfast, United Kingdom

[b] Department for Nanostructured Materials, Jožef Stefan Institute, Ljubljana, Slovenia

[c] Department of Industrial Chemistry "Toso Montanari", University of Bologna, Italy

[d] Department of Experimental Oncology, Institute of Oncology Ljubljana, Ljubljana, Slovenia

[e] University of Ljubljana, Faculty of Medicine, Institute of Cell Biology, Ljubljana, Slovenia

[f] School of Chemistry, University of East Anglia, Norwich Research Park, Norwich, United Kingdom

[g] Condensed Matter Physics Department, Jožef Stefan Institute, Ljubljana, Slovenia

[h] Department for Environmental Sciences, Jožef Stefan Institute, Ljubljana, Slovenia

*Corresponding author:
Dr Wafa' T. Al-Jamal
School of Pharmacy
Queen's University Belfast
Belfast, BT9 7BL
United Kingdom
E-mail: w.al-jamal@qub.ac.uk

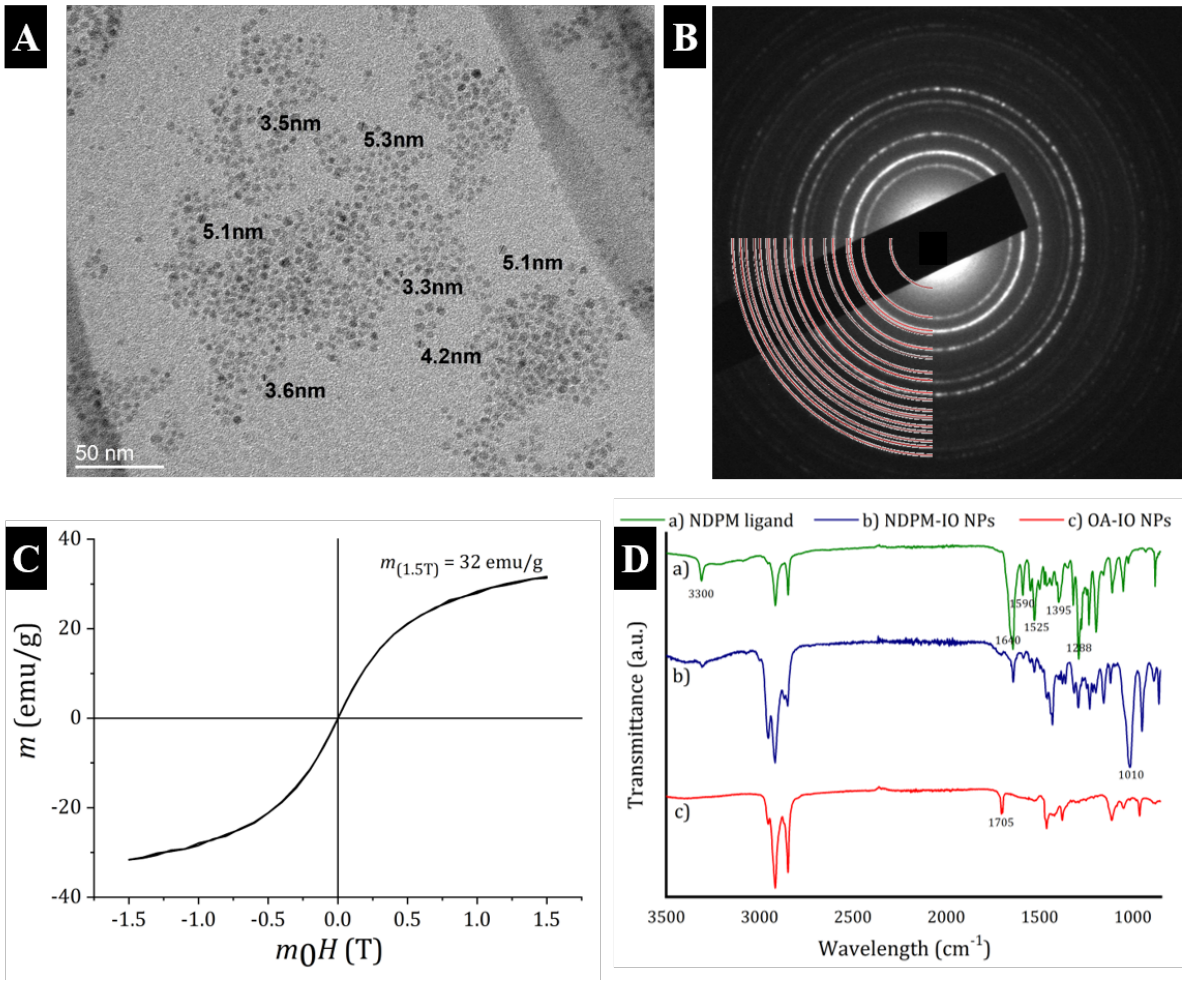

Figure S1. IO NPs characterisation. (A) TEM image and (B) corresponding SAED pattern indicating inverse spinel crystal structure. (C) Magnetic measurements of OA-coated IO NPs at 300 K. (D) Fourier-Transform Infrared Spectroscopy (FTIR) spectra of the soluble NDPM ligand, NDPM-coated IO NP and OA-coated IO NPs showing successful ligand exchange reaction.

A comparison of all three FTIR spectra (**Figure S1D**) revealed the successful exchange of the OA with the NDPM ligand on the surface of the IO NPs. The characteristic band at 1705 cm^{-1} for the C=O stretch of the hydrogen-bonded OA was not present in the FTIR spectrum for NDPM-coated IO NPs, which indicated complete ligand exchange. The following bands were present in both FTIR spectra for the pure NDPM ligand and the NDPM-coated IO NPs and, therefore, indicated the presence of the NDPM ligand on the surface IO NPs: band assigned to the asymmetric stretching of N-H bond (vas(N-H)) at 3300 cm^{-1}, the symmetric stretching of C=O at 1640 cm^{-1} and N-H bending at 1590 cm^{-1} confirmed the presence of the amide group, which was found in the NDPM ligand. Two strong bands representing N-O stretching of the NO2 group at 1525 and 1395 cm^{-1} and the band corresponding to the C-N stretching at 1288

cm^{-1} were also present, but the most prominent was the strong increase in the C-O stretching at 1110 cm^{-1} in the FTIR spectra for NDPM-coated IO NPs, indicating the binding of the NDPM ligand to the NP's surface [1], which was further confirmed by the reduction in the intensity of the C-O stretching of the catechol group ν(C-OH)aromatic at 1195 cm^{-1}.

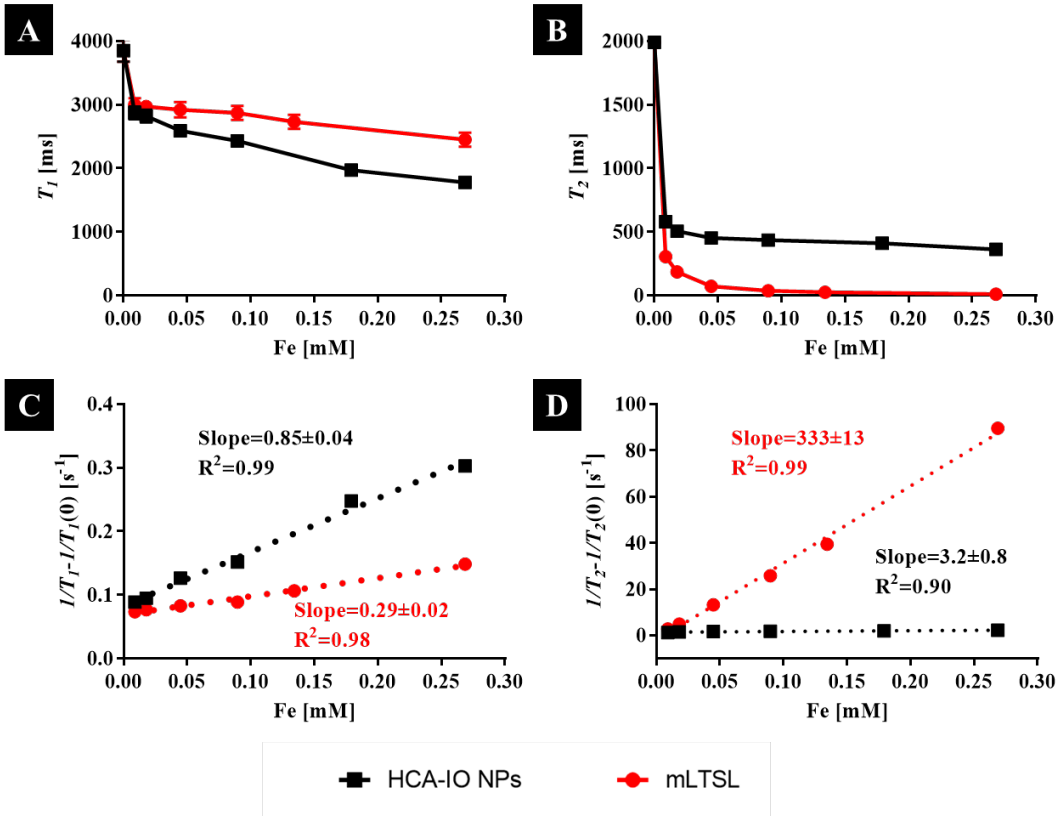

Figure S2. MRI properties of our developed mLTSL. (A) T_1 and (B) T_2 relaxation times of hydrophilic HCA-coated IO NPs and mLTSL with the corresponding (C) inverse longitudinal $1/T_1$ - $1/T_1(0)$ and (D) inverse transverse $1/T_2$ - $1/T_2(0)$ relaxation rate increase, where $T_1(0)$ and $T_2(0)$ represent the T_1 and T_2 relaxation times for water containing no particles.

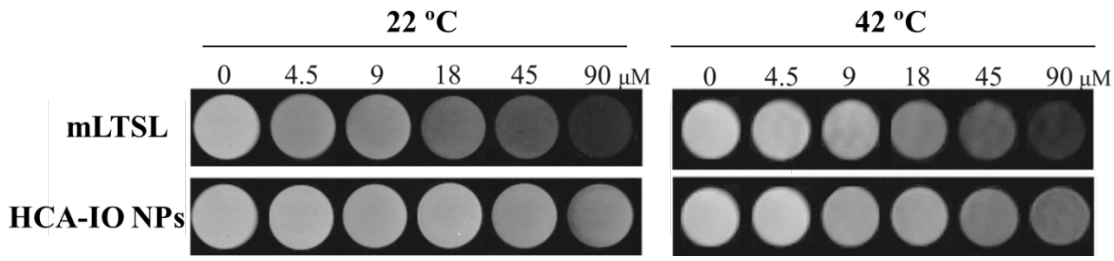

Figure S3. T_2**–weighted MRI images of hydrophilic HCA-coated IO NPs (bottom row) and mLTSL (top row) containing different concentrations of Fe at 22 and 42°C.**

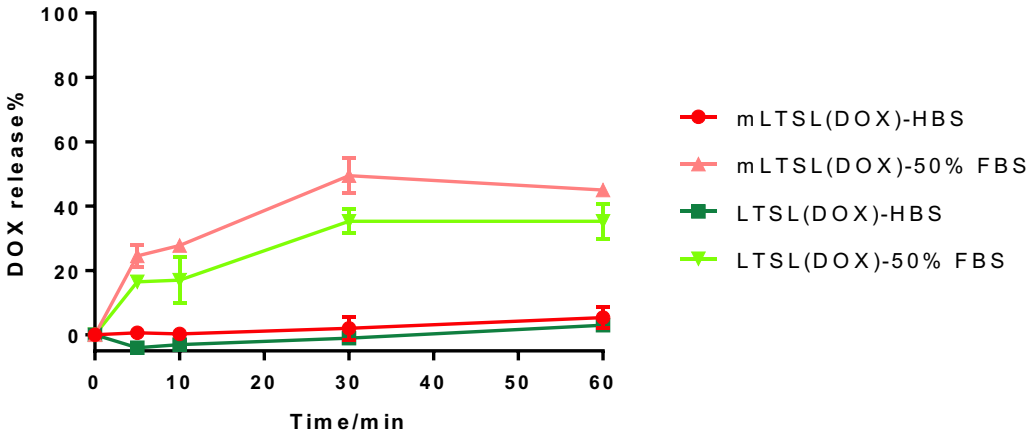

Figure S4. Serum stability of DOX-loaded mLTSL. DOX release profile of DOX-loaded LTSL and mLTSL ([Fe] = 20 μg/mL) at 37 ºC in HBS and 50% FBS**.**

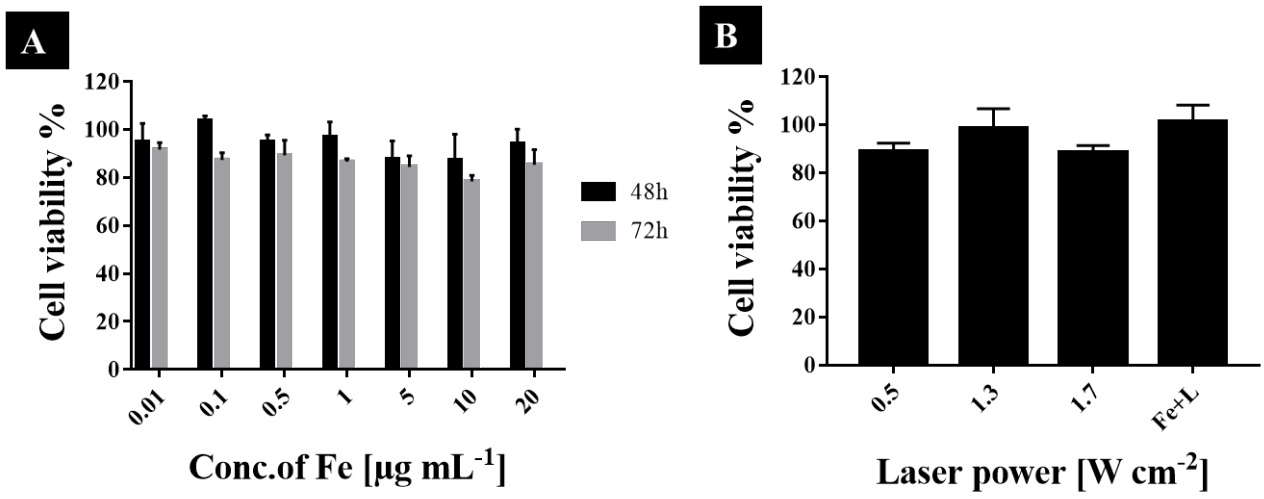

Figure S5. *In vitro* cytotoxicity of mLTSL. CT26 cells (1 x 10^4 /well) were seeded overnight in a 96 well-plate. Then cells were treated with (A) mLTSL containing different concentrations of Fe for 48 or 72 hours; (B) different laser powers (0.5, 1.3, 1.7 W/cm^2 for 5 min) and left for another 24 hours prior cell viability assay. CT26 cells were also added with mLTSL (20 µg/mL of Fe) in combination with laser (1.7 W/cm^2 for 5 min, Fe+L), and after 4 hours, cells were washed and replenished with fresh complete media, cell viability was assessed 20 hours later.

Table S1. Conjugation efficiency and physicochemical properties of anti-PD1-LTSL. Conjugation efficiency of anti-PD1 mAb to LTSL at different antibody-to-lipid ratios were characterized using BCA assay (BCA assay was carried out according to its protocol). Hydrodynamic size, polydispersity index (PDI) and zeta potential were determined using DLS.

Content of Maleimide	mAb/lipid [g/mol]	Conjugation efficiency (%)	Acquired mAb/lipid [g/mol]	Size±SD [nm]	PDI±SD	ζ potential ±SD [mV]
Mal (4%)-LTSL	NA	NA	NA	138±1.8	0.09±0.04	-12±2.4
Mal (4%)-LTSL	50	55	27.5	174.7±0.5	0.23±0.01	-7.95±1.92
Mal (2%)-LTSL	NA	NA	NA	139.7±2.2	0.07±0.03	-5.185±0.9
Mal (2%)-LTSL	100	18	18	164±4.1	0.14±0.01	-7.17±1.14
Mal (2%)-LTSL	50	32	16	156.9±5.4	0.17±0.1	-8.1±1.8

NA: not applicable

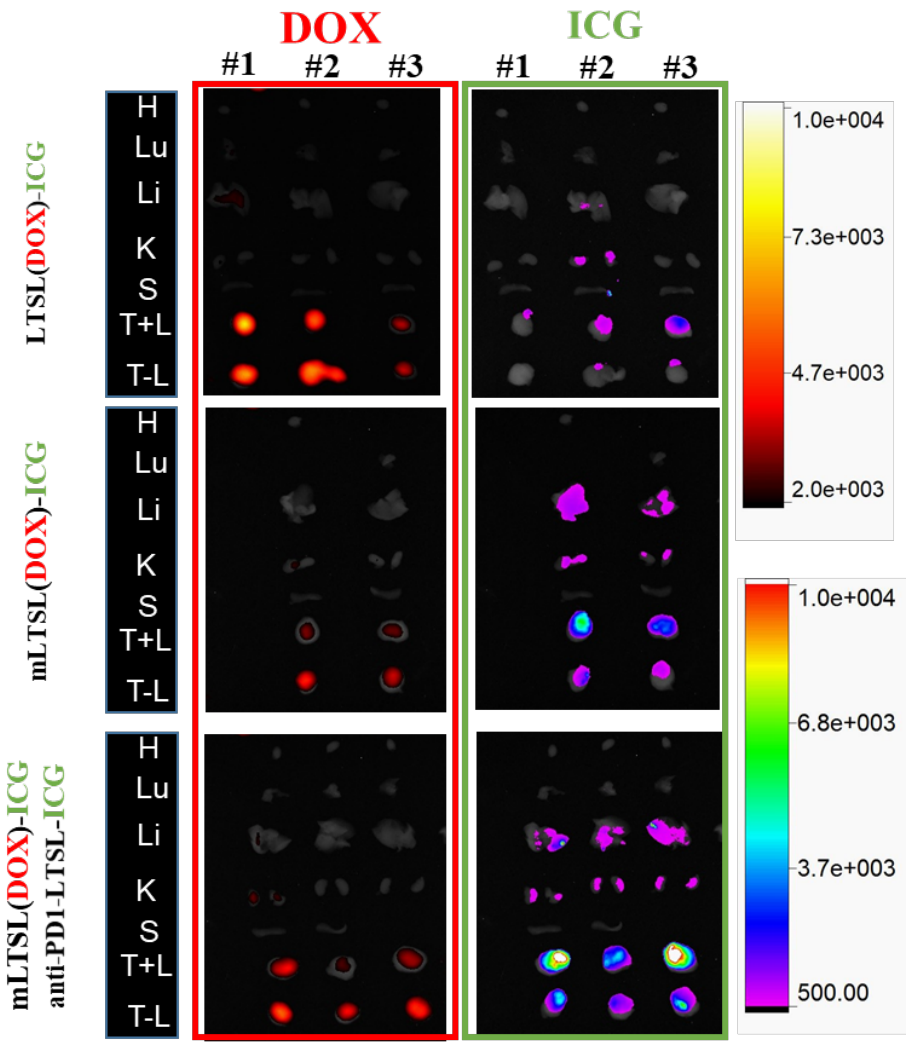

Figure S6. Organs accumulation of DOX-loaded mLTSL following intravenous administration and 808 nm laser irradiation. Mice injected with LTSL(DOX)-ICG, mLTSL(DOX)-ICG, and mLTSL(DOX)-ICG+anti-PD1-LTSL-ICG, were sacrificed after 24 hours and tumors and organs were collected for fluorescence imaging. DOX and ICG signals were detected in the isolated organs. H: heart, Lu: lung, Li: liver, K: kidney, S: spleen, T+L: tumour treated with laser (808 nm, 0.3 W/cm^2 for 10 min), T-L: tumor without laser treatment.

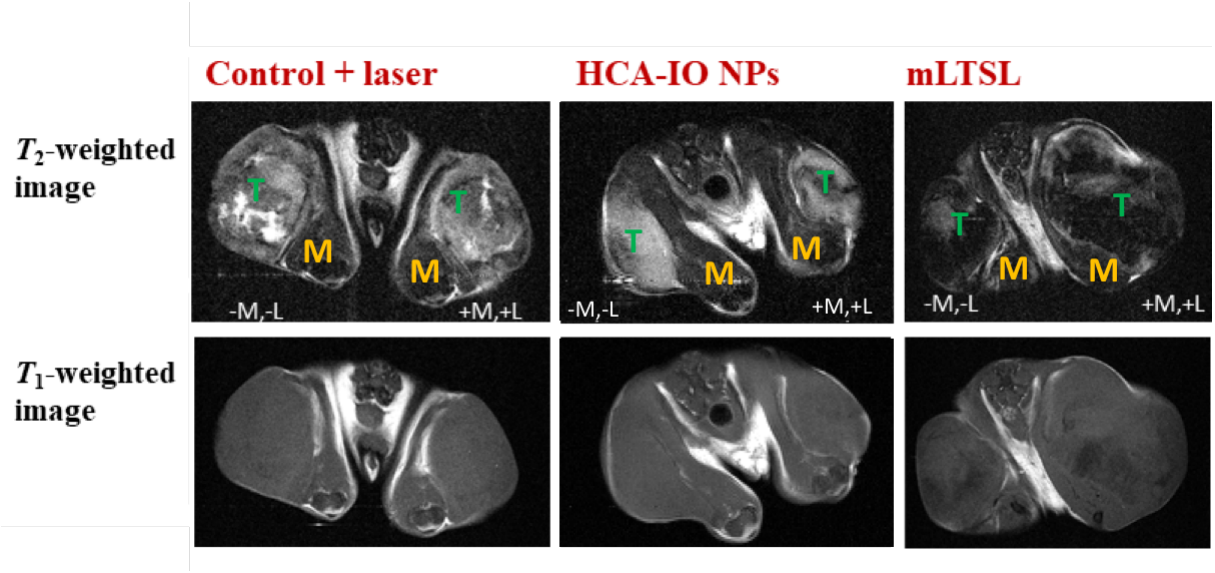

Figure S7. T_1- and T_2-weighted MR images recorded 24 hours post-injection. CT26 tumor-bearing mice were intravenously injected with PBS (control), HCA-IO NPs or mLTSL at a Fe dose of 50 µg per mouse. Tumors are indicated by (T) and normal muscle by (M). After injection, one tumor (implanted on the leg) was immediately taped with a magnet for 50 minutes (+M) and irradiated with the laser (808 nm, 0.3 W/cm^2) for 10 minutes (+L). The second tumor was not exposed to a magnet and was not irradiated (-M, -L). T_2-weighted images were taken 1 hour and 24 hours post-injection. T_1- and T_2-weighted MR images were recorded using the following sequences: TE/TR = 5/400 ms and TE/TR = 40/3000 ms, respectively.

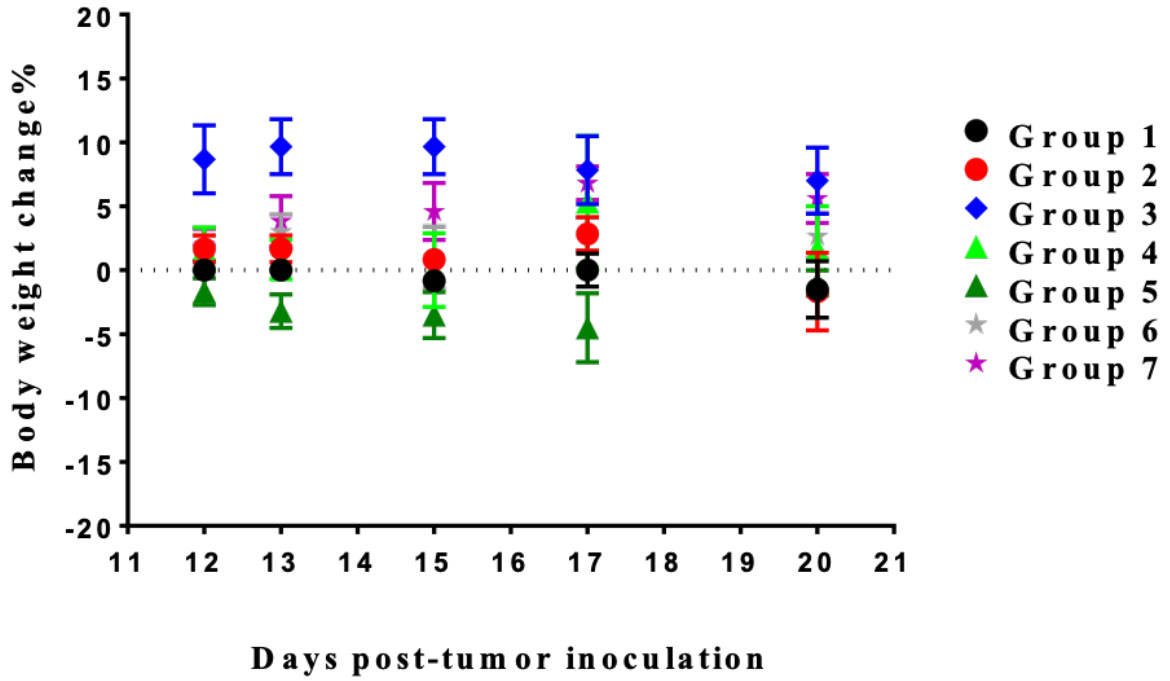

Figure S8. Changes in body weight of CT26-tumor bearing mice. Mice were intravenously injected with PBS (Group 1, control, black dots), free DOX (Group 2, 2 mg/kg, red dots), anti-PD1 mAb (Group 3, 2.5 mg/kg, blue diamonds), mLTSL(DOX) (Group 4, DOX: 2 mg/kg, Fe: 3 mg/kg, light green triangles), mLTSL (DOX)+anti-PD1-LTSL (Group 5, DOX: 2 mg/kg, Fe: 3 mg/kg, anti-PD1 mAb: 2.5 mg/kg, dark green triangles), LTSL (DOX) (Group 6, DOX: 2 mg/kg, grey stars), and anti-PD1-LTSL (DOX) (Group 7, DOX: 2 mg/kg, anti-PD1 mAb: 2.5 mg/kg, purple stars). After injection, one magnet disc was taped to the tumor and left for 50 minutes, then the tumors from all groups were irradiated with an 808 nm laser (0.3 W/cm^2 for 10 min). Body weight was monitored three times per week. Data are expressed as the mean ± SEM (n = 5).

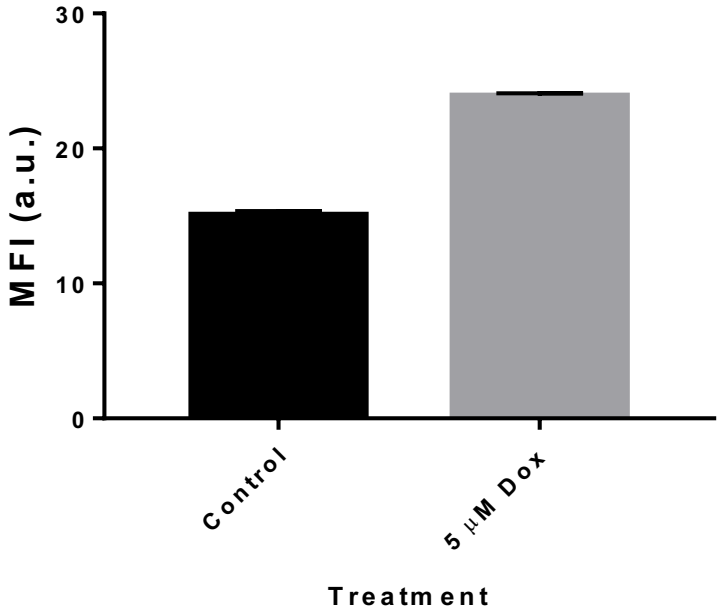

Figure S9: The expression of the ICD marker calreticulin on the surface of doxorubicin (Dox)-treated CT26 cells. CT26 cells were treated with 5 μM of Dox for 24 hours following which the expression of the ICD 'damage molecular pattern (DAMP)' calreticulin (CALR) was assessed on the surface of the treated cells against that of untreated CT26 populations. It was seen the 5 μM Dox treatment resulted in a ≈ 1.6-fold increase in CALR detection.

24-hours following the initiation of Dox treatment, both the treated CT26 cells and untreated CT26 cell populations, were incubated with anti-CALR rabbit antibodies (12238S, Cell Signalling), at a concentration of 1:600 in 0.5% BSA/ x1 PBS for 1 hour. The cells were harvested from culture wells mechanically using a syringe plunger to avoid the loss of surface proteins that is associated with trypsinization. Two thorough wash steps (1 mL 0.5 % BSA in PBS for 5 mins at 600g) were carried out between each antibody staining. Following the washing the cells were incubated with anti-rabbit AlexaFluor-594 conjugated secondary antibodies (88895, Cell Signalling) at a concentration of 1:1000 in 0.5% BSA/ x1 PBS for half an hour. FACs was carried out using a Becton Dickson FACSCaliber1 (BDbiosciences, Franklin lakes USA) following the manufactures instructions within the FL1 channel. Using the CellQuest FACs software (BDbiosciences, Franklin lakes USA) Geometric-mean fluorescent intensities (MFI) were compared between the Dox and untreated samples. Dead cells and debris were separated from viable cells via side and forward scatter and gated from the analysis. 10,000 viable gated cells were used for each sample; each treatment was repeated in triplicate.

REFERENCES

[1] E.D. Smolensky, H.-Y.E. Park, T.S. Berquó, V.C. Pierre, Surface functionalization of magnetic iron oxide nanoparticles for MRI applications - effect of anchoring group and ligand exchange protocol, Contrast Media Mol. Imaging, (2010) n/a-n/a, https://doi.org/10.1002/cmmi.417